Genomic analyses elucidate the causes and consequences of breakdown of distyly in *Linum trigynum*

Juanita Gutiérrez-Valencia[1], Panagiotis-Ioannis Zervakis[1], Zoé Postel[1], Marco Fracassetti[1], Aleksandra Losvik[1], Sara Mehrabi[1], Ignas Bunikis[2], Lucile Soler[3], P. William Hughes[1], Aurélie Désamoré[1], Benjamin Laenen[1], Mohamed Abdelaziz[4], Olga Vinnere Pettersson[2], Juan Arroyo[5], Tanja Slotte[1,*]

[1]Department of Ecology, Environment and Plant Sciences, Science for Life Laboratory, Stockholm University, Stockholm, Sweden

[2]Uppsala Genome Center, Department of Immunology, Genetics and Pathology, Uppsala University, Uppsala, Sweden

[3]Department of Medical Biochemistry and Microbiology, Uppsala University, National Bioinformatics Infrastructure Sweden (NBIS), Science for Life Laboratory, Uppsala University, Uppsala, Sweden

[4]Department of Genetics, University of Granada, Granada, Spain

[5]Department of Plant Biology and Ecology, University of Seville, Seville, Spain

*Corresponding author:

Tanja Slotte, Dept. of Ecology, Environment and Plant Sciences, Stockholm University, Stockholm SE-106 91 Stockholm, Sweden. Email: tanja.slotte@su.se

Running Title: Genomic analyses of breakdown of distyly in *Linum*

Key words: homostyly, self-fertilization, distribution of fitness effects, genome assembly, plant mating system.

Abstract

Distyly is an iconic floral polymorphism governed by a supergene, which promotes efficient pollen transfer and outcrossing through reciprocal differences in the position of sexual organs in flowers, often coupled with heteromorphic self-incompatibility (SI). Distyly has evolved convergently in multiple flowering plant lineages, but has also broken down repeatedly, often resulting in homostylous, self-compatible populations with elevated rates of self-fertilization relative to their distylous ancestors. Here, we aimed to study the causes and consequences of the shift to homostyly in *Linum trigynum*, which is closely related to distylous *Linum tenue.* Building on a high-quality genome assembly, we show that *L. trigynum* harbors a genomic region homologous to the dominant haplotype of the distyly supergene in *L. tenue*, suggesting that loss of distyly first occurred in a short-styled individual. In contrast to homostylous *Primula* and *Fagopyrum*, *L. trigynum* harbors no fixed loss-of-function mutations in coding sequences of *S*-linked distyly candidate genes. Instead, floral gene expression analyses and controlled crosses suggest that mutations downregulating the *S*-linked *LtWDR-44* candidate gene for male SI and/or anther height could underlie homostyly in *L. trigynum*. Population genomic analyses of 224 whole-genome sequences further demonstrate that *L. trigynum* is highly self-fertilizing, exhibits significantly lower genetic diversity genome-wide and is experiencing relaxed purifying selection on nonsynonymous mutations relative to *L. tenue*, despite the relatively recent split of *L. trigynum* and *L. tenue*. Our analyses elucidate the tempo and mode of loss of distyly in *L. trigynum*, and advances our understanding of a common evolutionary transition in flowering plants.

Introduction

Floral adaptations to different pollination modes have long fascinated evolutionary biologists (Darwin, 1876; 1877). One such adaptation is distyly, a floral polymorphism that promotes efficient pollen transfer and outcrossing via insect pollinators (Darwin, 1877; Lloyd & Webb 1992; reviewed by Barrett, 2019). Natural populations of distylous species are polymorphic for floral morph, such that individuals have one of two types of flowers that differ reciprocally in the positions of male and female sexual organs (anthers and stigmas, respectively) within the flower. Pin individuals have long styles (L-morph) and short stamens with stigmas at a high position and anthers at a low position in the flower, whereas thrum individuals have the reciprocal arrangement with short styles (S-morph) and long stamens (Fig. 1). In most distylous species, these morphological differences are coupled with a heteromorphic self-incompatibility (SI) system which allows inbreeding avoidance (Charlesworth and Charlesworth, 1979) and reinforces disassortative mating by preventing self- and intra-morph fertilization.

Despite its multi-trait nature, distyly is inherited as a single Mendelian locus, called the distyly supergene or the *S*-locus. The distyly supergene typically harbors two alleles: one dominant exclusive to thrums and one recessive for which pins are homozygous (Bateson and Gregory, 1905; Laibach, 1923) (Fig. 1). It is only recently that distyly supergenes have begun to be sequenced and characterized in detail (reviewed in Gutiérrez-Valencia et al., 2021). So far, characterization of independently evolved distyly supergenes in six systems (*Primula*: Li et al., 2016; *Turnera*: Shore et al., 2019; *Linum*: Gutiérrez-Valencia et al., 2022a; *Fagopyrum*: Yasui et al., 2012; Fawcett et al., 2023; *Gelsemium*: Zhao et al., 2023; *Nymphoides indica*: Yang et al., 2023) suggest a remarkable degree of convergence in the genetic architecture of distyly supergenes. Common features of independently evolved distyly supergenes include presence of indel variation and hemizygosity in thrum individuals, and similarities in patterns of molecular evolution (Gutiérrez-Valencia et al., 2022a).

While distyly has evolved independently at least 13 times in flowering plants (Naiki, 2012), it has broken down far more frequently, often resulting in homostylous species that are monomorphic and self-compatible (SC), with flowers harboring anthers and stigmas at the same height (reviewed by Ganders, 1979). Given their capacity for self-fertilization, homostylous individuals (homostyles) can be favored whenever insect-mediated pollination becomes unreliable, due to selection for reproductive assurance (e.g., Piper et al., 1986; Yuan et al., 2017). Genomic characterization of transitions from distyly to homostyly may therefore allow the identification of genetic changes underlying this mating system shift, as well as its population genomic consequences.

Because early models of the distyly supergene posited that thrum plants were heterozygous at the distyly supergene (Ernst, 1936), it was frequently hypothesized that rare recombination events between dominant and recessive *S*-haplotypes caused homostyly (Dowrick, 1956; Charlesworth and Charlesworth, 1979; reviewed by Ganders, 1979). This idea has been revisited after the realization that thrums are predominantly hemizygous rather than heterozygous at the distyly *S*-locus in several distylous systems (Li et al., 2016; Shore et al., 2019; Gutiérrez-Valencia et al., 2022a; Fawcett et al., 2023). Since hemizygosity precludes the possibility of recombination between the dominant and recessive haplotypes, other genetic

82 causes of distyly breakdown should be considered. First, unlinked genetic modifiers could act by reducing
83 floral herkogamy (Ganders, 1979; Mather & De Winton, 1941), precipitating distyly breakdown. Second,
84 distyly breakdown could be a consequence of loss-of-function mutations at *S*-linked genes (as suggested by
85 Ernst, 1936). Theory predicts that individuals that exhibit functional dominant male SI in combination with
86 recessive style length and female SI function should be favored during the establishment of homostyly
87 (Dowrick, 1956; Charlesworth and Charlesworth, 1979). In systems with hemizygous *S*-loci, it seems likely
88 that such combinations would arise by mutation and not recombination. So far, results on the breakdown of
89 distyly in *Primula* and *Fagopyrum* are in line with this prediction. In both systems, mutations affecting *S*-
90 linked genes responsible for female SI function and short styles (i.e., thrum-exclusive *CYP734A50* in
91 *Primula* and *S-ELF3* in *Fagopyrum*) can readily lead to the formation of long-homostylous SC plants,
92 because these *S*-linked genes jointly govern style length and female SI (Huu et al., 2016; Huu et al., 2022;
93 Fawcett et al., 2023). Moreover, independently evolved homostyles in natural populations of *Primula*
94 *vulgaris* harbor putative loss-of-function mutations in *CYP734A50* (Mora-Carrera et al., 2021). Mutations at
95 *S*-linked genes, particularly in genes affecting style length and female SI, thus constitute a feasible pathway
96 to loss of distyly, but it remains unknown if similar events have unfolded in other lineages of distylous
97 plants.

98 Genomic studies hold the promise to quantify the impact of homostyly on outcrossing rates, as well
99 as to characterize the consequences for patterns of polymorphism and the efficacy of selection. If the
100 evolution of homostyly is associated with shifts to high selfing rates, we expect the transition to result in
101 marked reductions in the effective population size (N_e), exacerbated by linked selection due to reduced
102 effective recombination rates in selfers, and potentially by founder events and bottlenecks associated with
103 selfing (reviewed by Wright et al., 2013; Slotte, 2014; Hartfield et al., 2017; Cutter, 2019). In combination,
104 these processes should result in reduced genetic diversity genome-wide, more marked population structure
105 and a decreased efficacy of selection, especially against weakly deleterious mutations, in selfing
106 homostylous species compared to their distylous relatives. Although transitions from distyly to homostyly
107 have occurred repeatedly in the history of flowering plants, the genomic consequences of this transition have
108 so far primarily been studied in one system, *Primula* (e.g., Wang et al., 2021, Zhong et al., 2019).

109 *Linum* is a promising system for studying the evolution and breakdown of distyly (e.g. Gutiérrez-
110 Valencia et al., 2022a), because it shows a remarkable diversity of stylar conditions, including several
111 independent losses of distyly (Ruiz-Martín et al., 2018; Maguilla et al., 2021). In agreement with the
112 expectation that selfers have improved colonization ability (Baker, 1955; Stebbins, 1957), phylogenetic
113 analyses suggest that the evolution of homostyly is associated with the expansion of *Linum* outside its center
114 of origin (Maguilla et al., 2021). It remains largely unknown how homostyly has emerged in *Linum*, but we
115 have recently shown that, similar to other distylous lineages, the distyly *S*-locus in *L. tenue* harbors a
116 hemizygous region exclusively inherited by thrums (Gutiérrez-Valencia et al., 2022a).

117 Here, we investigated the genetic causes and evolutionary consequences of loss of distyly in *Linum*
118 *trigynum*, an annual self-compatible species distributed across Spain and North Africa, in which homostyly
119 has been inferred as a derived state (Ruiz-Martín et al., 2018). For this purpose, we assembled and annotated

120 a high-quality genome sequence of the homostylous *L. trigynum* using PacBio high-fidelity (HiFi) long reads
121 and chromatin conformation capture (Hi-C) data. To investigate the genetic basis of loss of distyly, we
122 compared our *L. trigynum* genome assembly as well as two additional linked-read draft assemblies of *L.*
123 *trigynum* to eight genome assemblies of the closely related distylous species *L. tenue* (Gutiérrez-Valencia et
124 al., 2022a), with a focus on mutations and regulatory changes at *S*-linked genes. To characterize the timing
125 and mode of origin of homostyly, we analyzed polymorphism data based on 224 whole genome sequences
126 from eight natural populations each of *L. trigynum* and *L. tenue*. Finally, we conducted comparative
127 population genomic analyses to investigate the genome-wide effects of the shift to homostyly, in terms of
128 levels of diversity, inbreeding levels, population structure and the efficacy of purifying selection.
129

130 **Results**

131 *A Genomic Framework for Studying Breakdown of Distyly in Linum trigynum*

132 To provide a genomic framework for studies of the evolution of homostyly in *L. trigynum*, we generated a
133 high-quality *L. trigynum* genome assembly based on HiFi PacBio long reads (~41x coverage) and Hi-C data
134 from a single *L. trigynum* individual (see Materials and Methods and Table S1, Supplementary Information
135 for sample information). The resulting assembly was highly complete (complete BUSCOs=96.6%; Table S2,
136 Supplementary Information) and spanned 498 Mb (N50=47.03 Mb), divided in 10 chromosomes and five
137 scaffolds (less than 500 kb) with large-scale synteny to the *L. tenue* genome assembly (Gutiérrez-Valencia et
138 al., 2022a) (Fig. 2a, Fig. S1, Supplementary Information). Repetitive sequences constituted 56.49% of the
139 assembly, and we annotated a total of 54,692 coding genes, similar to the number in *L. tenue* (Gutiérrez-
140 Valencia et al., 2022a).

141 We supplemented our PacBio genome assemblies of *L. trigynum* and *L. tenue* with two additional
142 draft assemblies of *L. trigynum* based on 10x Chromium linked-read sequencing data (contig N50=4.82 Mb
143 vs 4.47 Mb; assembly size=461.69 Mb vs 463.46 Mb), and seven additional *L. tenue* linked-read assemblies
144 for thrum individuals which carry both the dominant and recessive haplotypes of the *S*-locus (Table S3,
145 Supplementary Information).
146

147 *Analyses of the* S*-locus Region Elucidate the Origin of Homostyly*

148 Whole-genome alignments of our high-quality *L. trigynum* and *L. tenue* assemblies showed that *L. trigynum*
149 carries a region on chromosome 10 that is homologous to the dominant haplotype of the *L. tenue* distyly *S*-
150 locus (Fig. 2b). Analyses of linked-read assemblies and genome coverage at this region based on short-read
151 data from 104 *L. trigynum* individuals further suggest that *L. trigynum* is fixed for the longer *S*-haplotype
152 that is dominant in *L. tenue* (Fig. 2c). Haplotype network analyses indicate that variation at the *L. trigynum*
153 *S*-locus stems from a single *S*-haplotype from its distylous ancestor (Fig. S2, Supplementary Information).
154 Together, these results suggest that events affecting the functioning of the supergene in thrum individuals led
155 to the breakdown of distyly, and that the haplotype identified in *L. trigynum* is likely derived from the
156 dominant *S*-haplotype.

157 We first investigated the gene content in the *L. trigynum* genome region homologous to the dominant
158 *S*-haplotype of *L. tenue*. After curation of *S*-locus annotation (see Materials and Methods for details), we
159 retained nine *S*-linked genes (Fig. 2d) in *L. tenue*. Out of these, five homologous *S*-linked genes were present
160 in our high-quality long-read *L. trigynum* assembly (Fig. 2d). These included the thrum-specific gene *LtTSS1*
161 which has pistil-specific expression and is likely to reduce cell length in thrum styles, and *LtWDR-44*
162 potentially involved in controlling anther position and/or pollen incompatibility in *L. tenue* (discussed in
163 Gutiérrez-Valencia et al., 2022a). In addition, *L. trigynum* harbored homologs of genes at the 5' end and 3'
164 ends of the *S*-locus region (Fig. 2d). The remaining genes, which are of unknown function (Gutiérrez-
165 Valencia et al. 2022a), were not present in the *L. trigynum* genome assembly (Fig. 2).
166 Next, we compared sequences of *L. tenue* and *L. trigynum* to identify candidate loss-of-function
167 changes at the *S*-locus region affecting gene function in *L. trigynum*, and to quantify synonymous and
168 nonsynonymous divergence between *L trigynum* and the dominant *S*-haplotype of *L. tenue.* We only
169 identified putative loss-of-function changes in *L. trigynum* in the gene *LtTSS1* (Table 1). This gene only
170 harbors one exon, as demonstrated by our updated annotation, validated by PCR-assays of cDNA structure
171 (see Materials and Methods for details; Fig. S3, Supplementary Information). In *LtTSS1*, we identified a C-
172 to-A mutation resulting in a premature stop codon in *L. trigynum* that was not fixed but segregating at a
173 frequency of 0.26 in our population data set, suggesting that it is unlikely to have initally caused loss of
174 distyly. Although all genes also harbored nonsynonymous mutations, there were no frameshift or other
175 major-effect mutations in the coding sequence of the other analyzed genes, nor markedly accelerated rates of
176 nonsynonymous substitution (Table 1).
177
178 *The* S-*linked Gene* LtWDR-44 *is Downregulated in Floral Buds of* L. trigynum
179 To determine if distyly breakdown in *L. trigynum* was associated with changes in transcript abundance at
180 candidate genes, we contrasted gene expression at *S*-linked genes in *L. tenue* thrums and *L. trigynum*
181 homostyles. We focused on detecting altered expression of any of the genes shared between the dominant *S*
182 allele of *L. tenue* and its derived allele fixed in *L. trigynum* (i.e., *liteg52183*, *indelg2*, *LtTSS1*, *LtWDR44* and
183 *LtTPR/liteg52188*). Out of these genes, only the stamen length and/or male SI candidate gene *LtWDR-44* was
184 significantly differentially expressed in floral buds, being downregulated in floral buds of *L. trigynum*
185 compared to *L. tenue* (Log_2-fold change = -1.58, $p < 0.01$, Fig. 3). *LtWDR-44* was not differentially
186 expressed between *L. tenue* thrums and *L. trigynum* homostyles in leaves (Supplementary Fig. S4;
187 Supplementary Information). None of the remaining *S*-linked genes showed significantly different levels of
188 expression in floral buds or leaves between *L. tenue* thrum and homostylous *L. trigynum* (Supplementary
189 Fig. S4; Supplementary Information).
190
191 *Pollination Assays Indicate Breakdown of Male SI in* L. trigynum
192 Distyly breakdown often evolves in association with loss of heteromorphic SI (reviewed by Barrett, 2019). If
193 the *S*-linked gene *LtWDR-44* is a determinant of male SI, as we previously hypothesized (Gutiérrez-Valencia
194 et al., 2022a), then we would expect downregulation of this gene to affect the male (pollen) SI expressed by

195 *L. trigynum*. Specifically, we would expect *L. trigynum* pollen to behave similarly to *L. tenue* pin pollen and
196 elongate successfully in thrum but not pin *L. tenue* pistils (Supplementary Fig. S5, Supplementary
197 Information). Crossing assays followed by pollen tube staining showed that *L. trigynum* grew long pollen
198 tubes in pistils of *L. tenue* thrum plants, but not in pistils of *L. tenue* pin plants (Fig. 3e, Supplementary Fig.
199 S5, Supplementary Information; note that for incompatible crosses, pollen tube rejection occurs in the style
200 in *Linum*; Murray 1986). These results are consistent with expectations if downregulation of *LtWDR-44* in *L.*
201 *trigynum* impairs male SI function.
202
203 *High Levels of Inbreeding in the Homostylous* L. trigynum
204 The fact that *L. trigynum* exhibits symptoms of the selfing syndrome in floral traits (Fig. 1) and has an
205 approximately fivefold lower pollen:ovule ratio compared to *L. tenue* (Repplinger, 2009) suggests that self-
206 pollination is likely to be its main mating strategy. If so, we would expect *L. trigynum* to be highly inbred.
207 To assess whether this was the case, we estimated the inbreeding coefficient using genome-wide
208 polymorphism data from 224 individuals representing eight populations per species (average n=14
209 individuals per population; Table S1, Supplementary Information). We found that estimates of the
210 inbreeding coefficient (F_{IS}) for *L. trigynum* were significantly higher than those for *L. tenue* populations
211 (Kruskal–Wallis test followed by Dunn's test with Benjamini-Hochberg adjustment of P-values, $P < 0.05$ for
212 all except two *L. trigynum – L. tenue* population comparisons; summary of median F_{IS} values across
213 populations: *L. tenue* mean=0.09, S.E.=0.03, n=8, *L. trigynum* mean=0.87, S.E.=0.04, n=8) (Fig. 4a).
214 Assuming equilibrium (Wright, 1969), the mean effective self-fertilization rate in *L. trigynum* is 0.93 ($2 F_{IS}$
215 $/[1+ F_{IS}]$). These results show that *L. trigynum* is more inbred than *L. tenue*, consistent with the shift to
216 homostyly and breakdown of SI resulting in elevated selfing rates.
217
218 *Stronger Population Structure and Reduced Polymorphism in* L. trigynum *Compared to* L. tenue
219 Transitions to self-fertilization are expected to result in reductions of the effective population size (N_e), and
220 thus reduced genetic diversity as well as more pronounced population structure in selfers relative to
221 outcrossers (Wright et al., 2013). To assess if the homostylous *L. trigynum* had reduced polymorphism levels
222 genome-wide compared to the distylous *L. tenue,* we obtained windowed estimates of nucleotide diversity
223 (π, 100 kb windows) for eight populations per species. In agreement with expectation, *L. trigynum* showed
224 markedly lower genome-wide π than *L. tenue* (Fig. 4b) (Kruskal–Wallis test followed by Dunn's test with
225 Benjamini-Hochberg adjustment of P-values, $P < 0.001$ for all *L. trigynum – L. tenue* populations
226 comparisons average π values across populations: *L. tenue*: mean=1.3×10^{-3}, S.E.=1.4×10^{-4}, n=8, *L. trigynum*:
227 mean=5.3×10^{-4}, S.E.=1.2×10^{-4}, n=8).
228 Next, we investigated population structure based on our genome-wide polymorphism (see Fig. 5a for
229 geographical origin of the sampled individuals). Structure analyses with ADMIXTURE, principal
230 component analyses (PCA), and TreeMix-based inference based on 76,934 SNPs in non-coding regions (see
231 Methods for details) showed that *L. tenue* and *L. trigynum* form clearly differentiated groups (Fig. 5b, c; Fig.
232 S6, Supplementary Information). We found the highest degree of differentiation between *L. tenue* and *L.*

233 *trigynum* populations (F_{ST} median=0.96, 1st and 3st quartile=0.95 and 0.97), followed by *L. trigynum* (F_{ST}
234 median=0.37, 1st and 3st quartile=0.28 and 0.50) and finally *L. tenue* (F_{ST} median=0.05, 1st and 3st
235 quartile=0.03 and 0.05) (Kruskal–Wallis test followed by Dunn's test with Bonferroni corrected *P* values, *P*
236 < 0.001) (Fig. S7, Supplementary Information). TreeMix analyses (Fig. 5c) further suggested the absence of
237 gene flow between *L. tenue* and *L. trigynum*, and stronger population structure within *L. trigynum* than in *L.*
238 *tenue*. Overall, these results show low population structure within *L. tenue*, and more marked population
239 structure within *L. trigynum* (Fig. 5b, c).
240 Finally, divergence population genomic analyses jointly estimating demographic parameters and
241 inbreeding levels suggested that the split between *L. tenue* and *L. trigynum* was relatively recent (about 340
242 kya) and associated with a marked effective population size reduction in *L. trigynum* (Fig. 5d) as well as
243 elevated inbreeding in *L. trigynum* (F_{IS} = 0.88). Together, these results suggest that the transition to
244 homostyly was associated with higher rates of self-fertilization and reduced N_e, and occurred within a
245 relatively recent evolutionary timeframe.
246
247 *Relaxed Purifying Selection Against Weakly Deleterious Mutations in* L. trigynum
248 Comparisons of highly selfing species and outcrossing relatives have repeatedly identified genome-wide
249 signatures of relaxed purifying selection in selfers (reviewed by Cutter, 2019). Here, we investigated if
250 similar patterns are observed in *L. trigynum*. First, we annotated repetitive regions in the genome sequences
251 of *L. trigynum* and *L. tenue*, and compared the proportion of transposable elements (TEs) in 50 kb windows.
252 Contrary to the expectation that selfing would allow the accumulation of harmful TEs insertions in the *L.*
253 *trigynum* genome after weakened selection due to reduced N_e (Charlesworth and Wright, 2001), we found no
254 significant differences in TE content of the genomes of these species (Fig. 4c) (t-test: t=1.49, df=20561,
255 *N.S.*).
256 We next investigated if the shift to selfing in *L. trigynum* has resulted in reduced efficacy of
257 purifying selection on nonsynonymous mutations, which could yield an elevated ratio of nonsynonymous to
258 synonymous polymorphism (π_N/π_S). In line with this expectation, we found that π_N/π_S estimates were slightly
259 higher in *L. trigynum* than in *L. tenue* (Fig. S8, Supplementary Information) (*L. tenue*: mean= 0.40, S.E.=
260 0.02, *n*=8, *L. trigynum*: mean= 0.50, S.E.= 0.15, *n*=8). To test if elevated π_N/π_S in *L. trigynum* was due to
261 weaker purifying selection, we estimated the distribution of negative fitness effects (DFE) of new
262 nonsynonymous mutations in each population of *L. trigynum* and *L. tenue* using fastDFE v1.0.0 (Fig. 4d). In
263 line with the expectation that reduced N_e in selfers should lead to relaxed selection against weakly
264 deleterious mutations (reviewed by Wright et al., 2013), we found that the proportion of new
265 nonsynonymous mutations that are effectively neutral was significantly higher in *L. trigynum* than in *L.*
266 *tenue* populations ($0 > N_es > -1$: median=0.442) compared to *L. tenue* ($0 > N_es > -1$: median=0.24) ($0 > N_es >$
267 -1: Wilcoxon rank-sum test, $P < 0.001$, *n*=8 populations per species), suggesting that selection against
268 weakly deleterious mutations is relaxed in *L. trigynum* relative to *L. tenue*. Moreover, we found a lower
269 proportion of new nonsynonymous mutations with moderate and strongly deleterious effects in *L. trigynum*
270 ($-1 > N_es > -10$: median=0.064, $-10 > N_es > -100$: median=0.074, $N_es < -100$: median=0.074) compared to *L.*

271 *tenue* (-1 > $N_e s$ > -10: median=0.096, and -10 > $N_e s$ > -100: median=0.132, $N_e s$ < -100: median=0.524)
272 (Wilcoxon rank-sum test, $P < 0.001$, n=8 populations per species). Together, these results show that the
273 efficacy of purifying selection on new nonsynonymous mutations is lower in *L. trigynum* than in *L. tenue*.
274

275 **Discussion**

276 Understanding the causes and consequences of major evolutionary transitions is an important aim in
277 evolutionary biology. The remarkable diversity of mating system strategies that plants exhibit provides an
278 opportunity to elucidate the causes of reproductive transitions, and how they impact the capacity of
279 populations to respond to selection. Here, we first generated a genomic framework to study genetic causes of
280 loss of distyly in *Linum*, and then used this framework to characterize the timing and mode of the transition
281 as well as its genomic consequences in terms of inbreeding levels, patterns of polymorphism, and the
282 efficacy of natural selection genome-wide.

283 While earlier models posited that rare recombination events between the recessive and dominant
284 alleles at the *S*-locus were the cause for distyly breakdown (Dowrick, 1956; Charlesworth and Charlesworth,
285 1979), recent findings have indicated that distyly *S*-loci harbor presence-absence variation and that thrums
286 are predominantly hemizygous at the *S*-locus rather than heterozygous (Li et al., 2016; Shore et al., 2019;
287 Gutiérrez-Valencia et al., 2022a; Fawcett et al., 2023; Yang et al., 2023; Zhao et al., 2023). The recent
288 characterization of the genetic architecture of the *S*-locus makes previous models of breakdown less likely
289 and rather indicates that mutations either at the *S*-locus or at unlinked modifier loci are more plausible causes
290 for the evolutionary shift from distyly to homostyly.

291 The presence of a genomic region in *L. trigynum* homologous to the thrum-specific dominant *S*-
292 haplotype of *L. tenue* strongly suggests that breakdown of distyly first occurred in a thrum individual. This
293 finding allowed us to identify candidate mutations for distyly breakdown, by comparing sequences of *S*-
294 linked genes in *L. tenue* and their homologues in *L. trigynum*. We also conducted differential expression
295 analyses between *L. trigynum* and *L. tenue* to determine if changes in the expression of *S*-linked genes might
296 have contributed to the evolution of homostyly in *L. trigynum.* Work in *Primula* (Huu et al., 2016; Huu et al.,
297 2022; Mora-Carrera et al., 2021) and *Fagopyrum* (Fawcett et al., 2023) has shown that shifts to homostyly in
298 both lineages were most likely precipitated by mutations at *S*-linked genes that simultaneously govern pistil
299 elongation and female SI. Although we found a premature stop codon in *LtTSS1,* which is a strong candidate
300 gene for style length and possibly female SI in *Linum* (Gutiérrez-Valencia et al., 2022a)*,* this major-effect
301 mutation was not fixed in *L. trigynum* populations, suggesting that loss of distyly has different genetic basis
302 in this species. Our differential expression analyses showed that *LtWDR-44,* which likely governs anther
303 position and/or pollen functioning, was the only *S*-linked gene downregulated in floral buds of *L. trigynum*
304 compared to *L. tenue*. Pollination assays further showed that *L. trigynum* pollen tubes can grow in styles of
305 *L. tenue* thrums but not in those of pins, consistent with expectations if downregulation of *LtWDR-44* in *L.*
306 *trigynum* disrupted the male component of the SI system. These results suggest that mutations resulting in
307 downregulation of the expression of *LtWDR-44* are a plausible cause of the breakdown of distyly in *L.*
308 *trigynum* via disruption of pollen SI, and should be subject to further functional study. Future studies could

309 expand our understanding of the breakdown of distyly in *L. trigynum* by investigating whether the alteration
310 of *LtWDR-44* might simultaneously disrupt male SI and contribute to decreased herkogamy, or if more
311 complex evolutionary pathways could have led to the evolution of homostylous flowers. Studies in *Turnera*
312 support the plausibility of this final scenario by showing that the *S*-linked *YUCG* gene determines the
313 functioning and size of pollen, but does not affect stamen length (Henning et al., 2022). Our finding of
314 downregulation of *LtWDR-44* associated with SC and a switch from thrum- to pin-type male SI in *L.*
315 *trigynum* constitutes an interesting contrast to the mode of loss of distyly in *Primula* and *Fagopyrum*, which
316 involved mutations at *S*-linked candidate genes for style length and female SI function (Huu et al., 2016;
317 Huu et al., 2022; Mora-Carrera et al., 2021, Fawcett et al., 2023).
318 Results from *Primula* and *Fagopyrum* are in line with theoretical predictions that long homostyles
319 harboring functional dominant male SI function in combination with recessive style length and female SI
320 function should be favored during establishment of homostyly (Dowrick, 1956; Charlesworth and
321 Charlesworth, 1979). Our findings so far do not conform to these theoretical expectations. It is possible that
322 this is the result of historical contingency. The early work by Dowrick (1956) showed that short homostyles
323 could increase in frequency in a distylous population, but they would do so at a slower rate than long
324 homostyles. However, short homostyles would still be expected to have an advantage over distylous
325 individuals under conditions that favor selfing. It is also possible that the function of *S*-locus genes in *Linum*
326 render a transition to homostyly via long homostyles more difficult than in *Primula*. Importantly, in the
327 absence of functional genetic studies of *LtTSS1* it remains uncertain whether loss-of-function mutations at
328 this gene could simultaneously alter both style length and female SI, as is the case in *Primula* (but see results
329 referring to the absence of *TSS1* in homostylous *L. lewisii* by Innes et al., 2023).
330 On the other hand, both theoretical work (Uyenoyama et al., 2001; Tsuchimatsu and Shimizu, 2013;
331 Shimizu and Tsuchimatsu, 2015) and empirical evidence (e.g., Tsukamoto et al., 2003; Tsuchimatsu et al.,
332 2010; Tsuchimatsu et al., 2012; Bachmann et al., 2019) have shown that mutations impacting male
333 components of the *S*-locus are a likely and common mechanism for transitions to SC in homomorphic SI
334 plant lineages. However, the loss of thrum-specific male SI does not instantly lead to compatibility with all
335 individuals in a distylous population, unlike the case of loss-of-function mutations in dominant *SCR* alleles
336 governing male SI in crucifers (e.g., Bachmann et al., 2019), so these two situations are not entirely
337 analogous. Studies in other clades will be required to determine how gene content at the *S*-locus and the
338 expression patterns of *S*-linked genes varies across distylous and homostylous species, and whether similar
339 genetic mechanisms are generally associated with distyly breakdown in *Linum*.
340 A caveat regarding the potential causes of loss of distyly in *L. trigynum* that we have identified is
341 that we cannot completely rule out a contribution of mutations at non-*S*-linked loci to reduced herkogamy
342 and SC in *L. trigynum* (Ganders, 1979; Mather and Winton, 1941). Unfortunately, such studies are precluded
343 here by the marked genome-wide differentiation between *L. trigynum* and *L. tenue* which prevents
344 identification of genetic variants associated with floral morph using association mapping. Additionally, we
345 were unable to obtain viable offspring from crosses of *L. trigynum* and *L. tenue*, preventing genetic mapping

346 in interspecific F2 mapping populations. Functional assays should instead be used to validate candidate
347 genetic changes that triggered loss of distyly in *L. trigynum.*
348 Transitions from distyly to homostyly are expected to frequently result in elevated self-fertilization
349 rates, with major consequences for genetic variation and the efficacy of selection. To elucidate the timeframe
350 within which the shift to homostyly occurred, as well as its genomic consequences, we analyzed 224 whole-
351 genome sequences of individuals from eight populations each of *L. trigynum* and *L. tenue*. We found that
352 homostyly was associated with predominant self-fertilization, and that the shift to homostyly occurred
353 relatively recently, within the approximately 340 ky since the split between *L. trigynum* and *L. tenue*. Despite
354 this relatively recent shift, there are already marked genomic consequences of self-fertilization. For instance,
355 our finding that *L. trigynum* is less genetically diverse and shows stronger population structure than *L. tenue*
356 are in line with some of the most frequently reported consequences of shifts to selfing (reviewed in Cutter,
357 2019).
358 Selfing is often associated with genome-wide relaxed purifying selection (Cutter, 2019). Here, we
359 assessed whether the genome of *L. trigynum* has accumulated TEs and deleterious mutations as a result of
360 reductions in N_e associated with selfing. Repetitive elements like TEs can duplicate and insert across the
361 genome with either neutral or deleterious effects (Quesneville, 2020), and thus they could increase in the
362 genome under weakened purifying selection (Charlesworth and Wright, 2001). On the other hand, selfers
363 could experience a reduction in TE content due to the efficient purging of recessive TE insertions with
364 deleterious fitness effects in selfers (Wright et al., 2008, Roessler et al., 2020). Our results suggest that
365 selfing in *L. trigynum* has not precipitated the accumulation of TEs compared to the outcrossing distylous *L.*
366 *tenue*. Studies conducted in other plant selfing lineages showed higher copy numbers of TEs per individual,
367 but accumulation patterns differed across TE families (Bonchev and Willi, 2018). Furthermore, the strength
368 of selection against TEs is expected to be especially strong if they interfere with genes or their regulatory
369 regions (reviewed by Quesneville, 2020; Horvath et al., 2017, Roessler et al., 2020). In consequence,
370 forthcoming analyses would benefit from exploring TE accumulation at a more refined scale by comparing
371 different TE families, and variation with respect to gene proximity.
372 Reductions in N_e resulting from bottlenecks and an increased impact of linked selection due to
373 elevated inbreeding are expected to result in reduced efficacy of selection against weakly deleterious
374 mutations in selfers (Wright et al., 2013; Burgarella & Glémin, 2017; Cutter, 2019). In line with this
375 prediction, we found evidence for weaker purifying selection in *L. trigynum* than in *L. tenue* based on
376 analyses of the distribution of fitness effects of new nonsynonymous (0-fold degenerate) mutations. With the
377 data at hand, we were unable to assess the full distribution of fitness effects, including positive selection, but
378 using improved outgroup genomes for reliable polarization future studies should address this question. In
379 addition, detailed analyses separately assessing selection on specific classes of genes, such as those involved
380 in the evolution of the selfing syndrome or pollen competition (Gutiérrez-Valencia et al., 2022b) would be
381 warranted for a more complete understanding of the impact of shifts to selfing on selection across the
382 genome. With these caveats, our analyses demonstrate genomic signatures consistent with relaxed selection
383 on nonsynonymous mutations in association with loss of distyly. These results are in line with previous

384 studies on the genomic impact of loss of distyly in *Primula* (Wang et al., 2021), and with a wealth of studies
385 on the genomic impact of shifts to selfing in other plant lineages (e.g., Slotte et al., 2010; Slotte et al., 2013;
386 Laenen et al., 2018; Mattila et al., 2020; Yi et al., 2022). Finally, comparative population genomic analyses
387 of multiple shifts from distyly to homostyly in *Linum* will be valuable to better understand general genomic
388 effects of this evolutionary transition.
389 Taken together, this study harnesses new genome assemblies, gene expression analyses, and
390 population genomic analyses to extend our understanding of the breakdown of distyly to a new system,
391 provide a basis for future research on the pathways associated with loss of distyly, and broaden our
392 knowledge on the evolutionary genomic consequences of shifts to selfing.
393

394 **Methods**

395 *Plant Material and Sequencing*

396 For genome sequencing and population genomic analyses, seeds and leaves of *L. trigynum* and *L. tenue* were
397 sampled in 16 different localities in southern Spain, representing 8 populations per species (Table S1,
398 Supplementary Information). Plants were grown in a controlled climate chamber at Stockholm University
399 (Stockholm, Sweden) set to 16 h light at 20°C: 8 h dark at 18°C, 60% maximum humidity, 122 µE light
400 intensity. We extracted DNA from 224 individuals for whole-genome short-read sequencing on an Illumina
401 NovaSeq 6000 on a S4 flowcell (150-bp paired-end reads, v1.5 sequencing chemistry). For long-read and
402 linked-read sequencing we extracted high molecular weight (HMW) DNA from young leaves using the
403 CTAB method (as in Fulton et al., 1995), followed by two purification steps with Genomic tip 500/G
404 (QIAGEN, Germany). To generate a high-quality genome assembly, HMW DNA of individual *Ltri*. 6-30-2
405 was sequenced on 2 Sequel II SMRT cells in HiFi mode, which led to the production of 27 Gb of HiFi data.
406 This was supplemented with Dovetail Hi-C sequencing data (OmniC) for the same individual. For linked-
407 read sequencing of two samples of *L. trigynum* (*Ltri.* 1-1-1 and *Ltri*. 1-42-2) and four samples of *L. tenue*
408 (*Lten*. CL-3-1, *Lten*. CL-75-1, *Lten*. STM-5-2, and *Lten.* STM-30-1) we used the Chromium Genome Library
409 preparation kit with sequencing on an Illumina HiSeqX system (paired-end 150bp read length, v2.5
410 sequencing chemistry). For genome annotation, we extracted total RNA from stems, leaves, floral buds, and
411 mature flowers of individual *Ltri*. 6-30-2, and for differential expression analyses, we extracted total RNA
412 from floral buds and leaves of *L. tenue* and *L. trigynum* (Sample size: *L. tenue* thrum=6, pin=4, *L. trigynum*
413 homostyle=5) using the RNeasy Plant Mini Kit (QIAGEN, Germany). Libraries were sequenced on an
414 Illumina NovaSeq S1 Sequencing System to produce paired-end 150bp read length reads. Full details on
415 plant growth, sampling, extraction and sequencing are given in Supplementary Methods, Supplementary
416 Information.
417

418 L. trigynum de novo *genome assemblies*

419 HiFi PacBio subreads were assembled with IPA (v1.3.2) (https://github.com/PacificBiosciences/pbipa) using
420 reads with QV20 or higher, which lead to a preliminary assembly of 103 primary contigs (total length =
421 498.60 Mb) and 2,280 associated contigs (total length = 100.57 Mb). To check for primary contigs that

422 should be identified as haplotigs we used Purge Haplotigs (Roach et al., 2018). Illumina short-reads obtained
423 from individual *Ltri*. 6-30-2 were mapped to the primary IPA assembly using minimap2 (Li, 2018), and the
424 alignments were processed with the function purge_haplotigs to generate a coverage histogram for contigs.
425 The resulting histogram showed a unimodal distribution, suggesting that purging was not required. The
426 assembly was scaffolded using Dovetail Hi-C data using 3D-DNA scaffolding (Dudchenko et al., 2017),
427 which was pre-filtered to only keep contacts with a mapping quality higher than 30. The expected haploid
428 number of chromosomes in *L. trigynum* is 10 (Pastor et al., 1990), and the resulting scaffolded assembly
429 consisted of 13 pseudochromosomes (N50 = 47.03 Mb, Length = 498.10 Mb). This assembly was further
430 edited to correct three misassemblies that were not supported by mapping of our PacBio reads to the *L.*
431 *trigynum* assembly. The edited *L. trigynum* genome assembly was polished two times with Pilon (Walker et
432 al., 2014) using Illumina short reads of the same individual. We screened the genome assemblly for regions
433 with high coverage and with similarity with the NCBI Plastid database
434 (https://www.ncbi.nlm.nih.gov/genome/organelle/). We detected and hard-masked one region with plastid
435 contamination on chromosome 6 (positions 59960001-60370000). We visualized broad-scale genome
436 synteny between our *L. tabrigynum* and *L. tenue* (Gutiérrez-Valencia et al., 2022a) assemblies by aligning
437 genome assemblies using minimap2 v2.4 (Li, 2018) and plotting alignments larger than 100 kb using the R
438 package circlize (Gu et al., 2014) (Fig. 2a).
439 Genomic linked-read sequences (10x Genomics) of two *L. trigynum* and four *L. tenue* samples were
440 assembled with the Supernova pipeline (https://github.com/10XGenomics/supernova) using default
441 parameters to obtain the output type pseudohap2. Furthermore we included three additional *L. tenue* linked-
442 read assemblies from Gutiérrez-Valencia et al. (2022a).
443
444 *Genome Annotation*
445 The annotation of *L. trigynum* was made with TSEBRA (Gabriel et al., 2021) which combines the gene
446 prediction of BRAKER1 (Hoff et al., 2015) and BRAKER2 (Brůna et al., 2021). BRAKER1 predicts genes
447 using RNAseq data, therefore we trimmed the raw reads from four different tissues (leaves, stems, floral
448 buds and mature flowers) with fastp (Chen et al., 2018), after we aligned them using STAR (Dobin and
449 Gingeras, 2015). BRAKER2 predict genes using protein databases, therefore we use protein data from *L.*
450 *tenue* (Gutiérrez-Valencia et al., 2022a) and four additional Malpighiales species (*L. usitatissimum*, *M.*
451 *esculenta*, *P. trichocarpa*, *S. purpurea*) download from phytozome (https://phytozome-next.jgi.doe.gov/)
452 (Goodstein et al., 2012). We used AGAT (https://github.com/NBISweden/AGAT) to extract the coding DNA
453 sequences needed to assess the genome completeness with BUSCO v5 (Manni et al., 2021). Repetitive
454 elements were identified using RepeatMasker (Smit et al., 2013) using a custom repeat library modelled
455 using RepeatModeler (Smit & Hubley, 2008).
456 We reannotated the *S*-locus genes in *L. tenue* and in *L. trigynum*. First, we identified the transcripts
457 with StringTie v2.1.4 (Pertea et al., 2015) using the RNA-seq data from (Gutiérrez-Valencia et al., 2022a).
458 Second, we predicted the proteins using TransDecoder v5.7.0 (https://github.com/TransDecoder/). Third, we
459 visually inspected the annotated genes using IGV v2.12.3 (Thorvaldsdóttir et al., 2012) retaining those well-

460 supported by RNA-seq evidence. In comparison to the previous *L. tenue* annotation (Gutiérrez-Valencia et
461 al., 2022a), two genes (*indelg1* and *LtTSS1*) were modified, leaving a total of nine genes at the dominant
462 allele of the *L. tenue S*-locus. Six genes with high similarity to repeats (*indelg3, indelg5, indelg6, indelg7,*
463 *indelg8, indelg9*) that were not analyzed in Gutiérrez-Valencia et al. (2022a) were not retained in our
464 updated annotation. In *L. trigynum* S-locus region we removed 22 genes annotated by TSEBRA because they
465 are not well-supported by RNA-seq evidence and we manually reannotated two genes (*indelg2* and *LtTSS1*)
466 in order to have the same intron-exon structure of the orthologs genes in *L. tenue*. Finally, we used NUCmer
467 (Kurtz et al., 2004) to identify orthologous regions between *L. tenue* and *L. trigynum* in the *S*-locus region
468 (Fig. 2d).
469

470 *Identification of Candidate Loss of Function* S-*Linked Mutations*

471 Using minimap2 (Li, 2018), we mapped the sequence of the *L. tenue* distyly *S*-locus (Gutiérrez-Valencia et
472 al., 2022a) against the genome assembly of *L. trigynum* to identify and extract the sequence homologous to
473 this region (Fig. 2b). The same approach was used to retrieve contigs containing the *S*-locus from 10X
474 genomics supernova assemblies (two *L. trigynum* and six *L. tenue.* We conducted BLAST analyses
475 (Camacho et al., 2009) to identify the sequences of *S*-locus genes in each assembly. Sequences of each gene
476 were independently aligned using MUSCLE v3.8.31 (Edgar, 2004), and only coding sequences were kept for
477 further analyses. Coding sequences were aligned using codon-aware alignment in webPRANK (Löytynoja
478 and Goldman, 2010). We inspected each alignment using AliView (Larsson, 2014) to identify major effect
479 mutations (non-consensus splice sites and premature stop codons). Estimates of mean synonymous (d_S) and
480 nonsynonymous divergence (d_N) between *L. tenue* and *L. trigynum* were obtained in MEGA X (Kumar et al.,
481 2018; Stecher et al., 2020) using the Nei-Gojobori model (Nei and Gojobori, 1986), with standard error
482 estimates obtained using 1000 bootstrap replicates. Ambiguous codon positions were removed for each
483 sequence pair.
484

485 *Sequence Processing, Mapping, Variant Calling and Filtering*

486 Illumina short reads from 224 individuals representing populations of *L. tenue* and *L. trigynum* were quality
487 and adaptor trimmed with *bbduk* from BBMap/BBTools (Bushnell, 2015). Trimmed paired-end reads were
488 mapped to the *L. tenue* genome assembly using BWA-MEM (v0.7.17) (Li, 2013). Alignments of *L. tenue*
489 and *L. trigynum* short reads to the *L. tenue* reference genome were used for coverage analyses focusing on
490 the *S*-locus region. For joint inference of demographic history and analyses of population structure, short-
491 read sequences of both species were mapped to the *L. tenue* genome assembly (Gutiérrez-Valencia et al.,
492 2022a). For all remaining analyses, sequences of each species were mapped to their corresponding reference
493 genome, and processed independently in downstream analyses leading to variant calling.
494 Alignments with mapping quality lower than 20 were discarded, and we used *MarkDuplicates* from
495 Picard tools v2.0.1 (Broad Institute, 2019) to remove duplicated reads from the alignment. The resulting
496 alignments were used to obtain genotype likelihoods with *mpileup*, and variants (SNPs/INDELs) and
497 invariant sites were identified by samtools/bcftools, using the model for multiallelic and rare-variant calling

498 (Danecek and McCarthy, 2017). The VCF file was processed to keep only biallelic SNPs and invariant sites,
499 and then filtered based on the maximum proportion of missing data (pm = 0.1) and read depth (5 < dp <
500 200). To avoid false heterozygous calls based on a low number of alternate alleles, we used a combination of
501 allele balance and coverage filtering, which has previously been successful for highly repetitive plant
502 genomes (see Laenen et al., 2018 and Gutiérrez-Valencia et al., 2022b for a detailed description).
503

504 *Coverage Analyses*

505 To investigate differences in depth of coverage between pin (n=25), thrum (n=26) (*L. tenue*) and homostyle
506 (n=104) (*L. trigynum*) at the *S*-locus, sequences mapped to both the *L. tenue* and *L. trigynum* genome
507 assemblies were processed to remove repetitive regions identified with RepeatMasker (Smit et al., 2013)
508 using the *L. usitatissimum* repeat library. We used BEDTools (Quinlan et al., 2010) to estimate coverage for
509 50 kb windows across the genome. Estimates were further processed using in R to estimate normalized mean
510 coverage across windows, and differences between morphs were tested using a Kruskal-Wallis test, followed
511 by a post-hoc Dunn's test with Bonferroni correction for multiple testing.
512

513 *Haplotype Network Analyses*

514 To investigate whether loss of distyly in *L. trigynum* might have occurred repeatedly, we conducted a
515 haplotype network analysis of two genes at the *S*-locus, *LtTSS1* and *LtWDR-44*. We used the genome
516 annotations of *L. tenue and L. trigynum* species to extract coding sequences for these two genes. We then
517 extracted the corresponding sequences from our short-read data using bam2consensus, a tool from the
518 package tool bambam v.1.4 (Page et al., 2014). In total, 67 *L. tenue* and 100 *L. trigynum* individuals had
519 sufficient coverage and were included in this analysis. We aligned all sequences using codon-aware
520 alignment in PRANK (Löytynoja and Goldman, 2010). Haplotypes and haplotype network were assessed
521 using the R package pegas v.1.2 (Paradis, 2010).
522

523 *Differential Expression Analyses*

524 RNASeq raw reads from floral buds and leaves were processed with the function bbduk from
525 BBMap/BBTools (Bushnell, 2015) for quality and adapter trimming (parameters k=2, mink=11, ktrim=r,
526 minlength=50, qtrim=rl, trimq=20, hdist=1, tbo, tpe). Reads were mapped and quantified with STAR (Dobin
527 and Gingeras, 2015), using the genome reference and the longest isoform per transcript from our updated
528 annotation of *L. tenue*. Multimapping reads were discarded by using the flag outFilterMultimapNmax=1.
529 Files listing counts mapped to each feature (ReadsPerGene.out.tab) were further processed in R to conduct
530 differential expression analyses using the package DESeq2 (Love, Huber and Anders, 2014). Two
531 independent contrasts were conducted for floral buds and leaves separately: homostyles were first contrasted
532 to thrums, and then to pins. We corrected for multiple testing with the Benjamini-Hochberg method, and
533 genes with an adjusted Log2-fold change > |1.5| and $p < 0.01$ were considered significantly differentially
534 expressed.
535

536 *Pollination Assays*

537 To test the functionality of male and female SI in *L. trigynum*, we conducted controlled reciprocal crosses of
538 *L. trigynum* (*n*=2 individuals) to both pin (*n*=2-5) and thrum (*n*=2-4) morphs of *L. tenue.* For comparison we
539 also conducted self-pollination of *L. trigynum*, compatible (pin x thrum, thrum x pin) and incompatible
540 pollinations (thrum x thrum, pin x pin) in *L. tenue* and negative controls without pollination. We did three
541 technical replicates of each type of cross of two individuals. For pollination, whole pistils were removed
542 from mature flower buds or recently opened flowers, placed on agar plates and hand pollinated. Pollen tube
543 growth was observed after 4 h. For pollen tube staining, we adapted a protocol by (Mori et al. 2006).
544 Specifically, hand-pollinated pistils were fixed with 9:1 ethanol: acetic acid solution 4 hours after
545 pollination. Pistils were then hydrated with an ethanol series (70%, 50% and 30% ethanol) and softened
546 overnight in 1 M NaOH. Pollen tube growth was observed under an UV fluorescence microscope (Olympus
547 BX60) after staining with 0.1% (w/v) aniline blue solution in 100 mM K_3PO_4 and 2% glycerol.

548

549 *Population Structure and Timing of Split*

550 The filtered VCF was pruned based on linkage disequilibrium (r^2) prior to conducting structure and
551 demographic analyses with PLINK (Chang et al., 2015) (parameters: window size in kilobase=50, variant
552 count to shift the window at the end of each step=5, pairwise r^2 threshold=0.5). We used the function *--pca*
553 also implemented in PLINK (Chang et al., 2015) to conduct a Principal Component Analysis (PCA) on SNPs
554 in the pruned VCF. The same data set was used for the structure analysis in ADMIXTURE (Alexander et al.,
555 2009) using values of *K* ranging from 2 to 16. The most likely number of subpopulations in the population
556 was determined after identifying the *K* value with the lowest cross-validation error. The results of both the
557 PCA and structure analyses were plotted in R (R Core Team, 2021). Weighted F_{ST} values were calculated
558 using the Weir and Cockerham estimator (Weir & Cockerham, 1984) implemented in VCFTools using the
559 function *--weir-fst-pop* (Danecek et al., 2011). Pairwise F_{ST} values were then compared within and between
560 species using a Kruskal–Wallis test followed by Dunn's test , and *P*-values were corrected using the
561 Bonferroni method in R (R Core Team, 2021). We investigated historical relationships among populations
562 using TreeMix (Pickrell and Pritchard, 2012) with 0 to 5 migration edges, running 100 iterations to get the
563 optimal number of migration edges. Using the evanno method implemented in the R package OptM (Evanno
564 et al., 2005; Fitak, 2021), we got an optimum of two migration edges, which were between populations of *L.*
565 *trigynum*. We further ran 60 iterations with two migration edges to ensure we had the maximum likelihood
566 tree, as well as 1000 bootstrap replicates to obtain confidence intervals. No admixture was detected between
567 the species. Finally, we used an extension of *dadi* (Gutenkunst et al., 2009) by Blischak et al. (2020) to
568 coestimate inbreeding and demographic parameters of a simple split model for *L. tenue* and *L. trigynum*. For
569 simplicity, we only included one population each of *L. tenue* and *L. trigynum* (populations 32 and 11,
570 respectively) in this analysis.

571

572 *Estimates of Inbreeding and Polymorphism*

We estimated the inbreeding coefficient (F_{IS}) (Wright, 1951) to assist our understanding of the prevalence of selfing in *L. trigynum* using the option *--het* in VCFTools (Danecek et al., 2011). Nucleotide polymorphism (π) was estimated in 100 kb windows per population using pixy (Korunes and Samuk, 2021). Statistical testing for significant differences in F_{IS} and windowed π across populations was conducted in R (R Core Team, 2021).

Estimates of Purifying Selection

To compare the content of TEs between the genomes of *L. tenue* and *L. trigynum*, we created custom libraries of repeats using RepeatModeler (Smit and Hubley, 2008). The resulting libraries were then used to identify loci harboring these repeats using RepeatMasker (Smit et al., 2013). We divided genome sequences in 50 kb windows using BEDTools (Quinlan and Hall, 2010), and estimated the proportion of TEs per window in R (R Core Team, 2021).

We investigated purifying selection at coding sequences using the annotation of both *L. tenue* (Gutiérrez-Valencia et al., 2022a) and *L. trigynum*. We calculated π_N/π_S using pixy with the options *--bed_file* and *--sites_file* to estimate π on a per-gene basis and by restricting the analyses to 0-fold and 4-fold sites. π_N and π_S were computed in R to obtain and compare values of π_N/π_S. These sites were identified using the python script NewAnnotateRef.py (https://github.com/fabbyrob/science/tree/master/pileup_analyzers) (Williamson et al., 2014) ran separately on our annotated high-quality long-read *L. tenue* and *L. trigynum* assemblies, considering only the longest transcript per gene. Finally, estimates of DFE for each population were obtained using fastdfe (v1.0.0) (https://github.com/Sendrowski/fastDFE), a python implementation of polyDFE (Tataru et al., 2017) which supports deleterious DFE inference from folded frequency spectra. We used the model "GammaExpParametrization" which models the DFE under a Γ distribution. In the model, we parametrized the folded SFS using the nuisance parameters with the option "get_demography" to account for demographic history effects. Since we did not have divergence information, we could only obtain the deleterious DFE by setting "p_b=0", while other models provided are equivalent for that purpose. We ran 200 iterations to get the highest maximum likelihood fit, while confidence intervals were obtained with 300 bootstrap replications. As before, 0-fold degenerate sites were considered to be under stronger purifying selection than 4-fold degenerate sites which were assumed to evolve neutrally. Site frequency spectra for 0- and 4-fold sites were obtained with easySFS (https://github.com/isaacovercast/easySFS) which uses a modified implementation of *dadi* (Gutenkunst et al., 2009) with the option "-a" to keep all SNPs. DFE results were summarized in four bins depicting the proportion of new mutations evolving as effectively neutral ($0 > N_e s > -1$), moderately ($-1 > N_e s > -10$), and strongly deleterious ($-10, N_e s > -100$) and ($-100 > N_e s$). The proportion of mutations in each category was compared between species using R (R Core Team, 2021).

Data Availability

All sequencing data, genome assemblies and their annotation produced in this study has been uploaded to the European Nucleotide Archive (ENA) (https://www.ebi.ac.uk/ena/) under study accession number PRJEB67577.

Acknowledgments

We thank José Ruíz-Martin for assistance with field work, Jerker Eriksson for technical assistance, and Björn Nystedt for discussion of the project. This project has received funding from the European Research Council (ERC) under the European Union's Horizon 2020 research and innovation programme (grant agreement No 757451), from the Swedish Research Council (grant no. 2019-04452) and the Erik Philip-Sörensen foundation to T.S., and from the Bergströms foundation to J.G.V., and from the Nilsson-Ehle foundation to P.W.H. Z.P. is financially supported by a Carl Tryggers fellowship (CTS 21:1471). The authors acknowledge support from the National Genomics Infrastructure (NGI) in Stockholm and Uppsala (Uppsala Genome Center, SNP&SEQ), funded by the Knut and Alice Wallenberg foundation, the Swedish Research Council and Science for Life Laboratory. We acknowledge support of the Swedish National Infrastructure for Computing (SNIC) and Uppsala Multidisciplinary Center for Advanced Computational Science (UPPMAX) for assistance with massively parallel sequencing and access to computational infrastructure. Support by NBIS (National Bioinformatics Infrastructure Sweden) is gratefully acknowledged.

References

Alexander, D. H., Novembre, J., & Lange, K. (2009). Fast model-based estimation of ancestry in unrelated individuals. *Genome Research*, *19*, 1655–1664.

Bachmann, J. A., Tedder, A., Laenen, B., Fracassetti, M., Désamoré, A., Lafon-Placette, C., Steige, K. A., Callot, C., Marande, W., Neuffer, B., Bergès, H., Köhler, C., Castric, V. and Slotte, T. (2019). Genetic basis and timing of a major mating system shift in *Capsella*. *New Phytologist*, *224*, 505-517.

Baker, H. G. (1955). Self-compatibility and establishment after "long-distance" dispersal. *Evolution*, *9*, 347–349.

Barrett, S. C. H. (2019). 'A most complex marriage arrangement': Recent advances on heterostyly and unresolved questions. *New Phytologist*, *224*, 1051–1067.

Bateson, W., & Gregory, R. P. (1905). On the inheritance of heterostylism in *Primula*. *Proceedings of the Royal Society B: Biological Sciences*, *76*, 581–586.

Blischak, P. D., Barker, M. S., Gutenkunst, R. N. (2020). Inferring the demographic history of inbred species from genome-wide SNP frequency data. *Molecular Biology and Evolution*, *37*, 2124–2136.

Bonchev, G., Willi, Y. (2018). Accumulation of transposable elements in selfing populations of *Arabidopsis lyrata* supports the ectopic recombination model of transposon evolution. *New Phytologist*, *219*, 767–778.

Broad Institute. (2019). Picard Tools. *Broad Institute, GitHub Repository*. http://broadinstitute.github.io/picard/

Brůna, T., Hoff, K. J., Lomsadze, A., Stanke, M., Borodovsky, M. (2021). BRAKER2: automatic eukaryotic genome annotation with GeneMark-EP+ and AUGUSTUS supported by a protein database. *NAR Genomics and Bioinformatics*, *3*, lqaa108.

Burgarella, C., & Glémin, S. (2017). Population genetics and genome evolution of selfing species. In *ELS* (pp. 1–8). John Wiley & Sons, Ltd.

Bushnell, B. (2015). *BBMap/BBTools*. sourceforge.net/projects/bbmap/

Camacho, C., Coulouris, G., Avagyan, V., Ma, N., Papadopoulos, J., Bealer, K., & Madden, T. L. (2009). BLAST+: Architecture and applications. *BMC Bioinformatics*, *10*, 421.

Chang, C. C., Chow, C. C., Tellier, L. C., Vattikuti, S., Purcell, S. M., Lee, J. J. (2015). Second-generation PLINK: Rising to the challenge of larger and richer datasets. *GigaScience*, *4*, s13742–015–0047–8.

Charlesworth, D., Charlesworth, B. (1979). A model for the evolution of distyly. *The American Naturalist*, 114(4), 467–498.

Charlesworth, D., Wright, S. I. (2001). Breeding systems and genome evolution. *Current Opinion in Genetics & Development*, *11*, 685–690.

Chen, S., Zhou, Y., Chen, Y., Gu, J. (2018). fastp: an ultra-fast all-in-one FASTQ preprocessor. *Bioinformatics*, *34*, i884-i890.

Cutter, A. D. (2019). Reproductive transitions in plants and animals: Selfing syndrome, sexual selection and speciation. *New Phytologist*, *224*, 1080–1094.

Danecek, P., Auton, A., Abecasis, G., Albers, C. A., Banks, E., DePristo, M. A., Handsaker, R. E., Lunter, G., Marth, G. T., Sherry, S. T., McVean, G., & Durbin, R. (2011). The variant call format and VCFtools. *Bioinformatics*, *27*, 2156–2158.

Danecek, P., & McCarthy, S. A. (2017). BCFtools/csq: Haplotype-aware variant consequences. *Bioinformatics, 33*, 2037–2039.

Darwin, C. (1876). *The Effects of Cross and Self Fertilisation in the Vegetable Kingdom*. Cambridge University Press; Cambridge Core.

Darwin, C. (1877). The effects of cross and self fertilisation in the vegetable kingdom. Cambridge University Press; Cambridge Core.

Dobin, A., Gingeras, T.R. (2015). Mapping RNA-Seq reads with STAR. Current Protocols in Bioinformatics, 51, 11.14.1-11.14.19.

Dowrick, V. P. J. (1956). Heterostyly and homostyly in *Primula obconica*. *Heredity*, *10*, 219–236.

Dudchenko, O., Batra, S. S., Omer, A. D., Nyquist, S. K., Hoeger, M., Durand, N. C., Shamim, M. S., Machol, I., Lander, E. S., Aiden, A. P., & Aiden, E. L. (2017). *De novo* assembly of the *Aedes aegypti* genome using Hi-C yields chromosome-length scaffolds. *Science*, *356*, 92–95.

Edgar, R. C. (2004). MUSCLE: multiple sequence alignment with high accuracy and high throughput. *Nucleic Acids Research*, *32*, 1792–1797.

Ernst, A. (1936). Heterostylie-Forschung. *Zeitschrift für Induktive Abstammungs- und Vererbungslehre*, *71*, 156–230.

Evanno, G., Regnaut, S., Goudet, J. (2005). Detecting the number of clusters of individuals using the software STRUCTURE: a simulation study. *Molecular Ecology*, *14*, 2611–20.

Fawcett, J.A., Takeshima, R., Kikuchi, S. *et al.* (2023). Genome sequencing reveals the genetic architecture of heterostyly and domestication history of common buckwheat. *Nature Plants*, 9, 1236–1251.

Fitak, R. R. (2021). *OptM*: estimating the optimal number of migration edges on population trees using Treemix. Biology Methods and Protocols, 6, bpab017.

Fulton, T. M., Chunwongse, J., & Tanksley, S. D. (1995). Microprep protocol for extraction of DNA from tomato and other herbaceous plants. *Plant Molecular Biology Reporter*, *13*, 207–209.

Gabriel, L., Hoff, K.J., Brůna, T. et al. (2021). TSEBRA: transcript selector for BRAKER. BMC *Bioinformatics*, *22*, 566

Ganders, F. R. (1979). The biology of heterostyly. *New Zealand Journal of Botany*, *17*, 607–635.

Goodstein, D. M., Shu, S., Howson, R., Neupane, R., Hayes, R. D., Fazo, J., Mitros, T., Dirks, W., Hellsten, U., Putnam, N., Rokhsar, D. S. (2012). Phytozome: a comparative platform for green plant genomics. *Nucleic Acids Research*, *40*, D1178-1186.

Gu, Z., Gu, L., Eils, R., Schlesner, M., Brors, B. (2014). Circlize implements and enhances circular visualization in R. *Bioinformatics*, 19, 2811–2812.

Gutenkunst, R. N., Hernandez, R. D., Williamson, S. H., & Bustamante, C. D. (2009). Inferring the joint demographic history of multiple populations from multidimensional SNP frequency data. *PLOS Genetics*, 5, e1000695.

Gutiérrez-Valencia, J., Hughes, P.W., Berdan, E.L., &Slotte, T. (2021). The genomic architecture and evolutionary fates of supergenes. *Genome Biology and Evolution*, *13*, evab057.

Gutiérrez-Valencia, J., Fracassetti, M., Berdan, E. L., Bunikis, I., Soler, L., Dainat, J., Kutschera, V. E., Losvik, A., Désamoré, A., Hughes, P. W., Foroozani, A., Laenen, B., Pesquet, E., Abdelaziz, M., Pettersson, O. V., Nystedt, B., Brennan, A. C., Arroyo, J., & Slotte, T. (2022a). Genomic analyses of the *Linum* distyly supergene reveal convergent evolution at the molecular level. *Current Biology*, *32*, 4360-4371.

Gutiérrez-Valencia, J., Fracassetti, M., Horvath, R., Laenen, B., Désamore, A., Drouzas, A.D., Friberg, M., Kolár, F., & Slotte, T. (2022b). Genomic signatures of sexual selection on pollen-expressed genes in *Arabis alpina*. *Molecular Biology and Evolution*, 39, msab349.

Henning, P. M., Shore, J. S., McCubbin AG. (2022). The S-gene YUC6 pleiotropically determines male mating type and pollen size in heterostylous Turnera (Passifloraceae): a novel neofunctionalization of the yucca gene family. *Plants*, 11, 2640.

Hartfield, M., Bataillon, T., & Glémin, S. (2017). The evolutionary interplay between adaptation and self-fertilization. *Trends in Genetics*, *33*, 420–431.

Hoff, K. J., Lange, S., Lomsadze, A., Borodovsky, M., Stanke, M. (2016). BRAKER1: unsupervised RNA-Seq-based genome annotation with GeneMark-ET and AUGUSTUS. *Bioinformatics*, *32*, 767–769.

Horvath, R., Slotte, T. 2017. The role of small RNA-based epigenetic silencing for purifying selection on transposable elements in *Capsella grandiflora*. *Genome Biology and Evolution*, *9*, 2911-2920.

Huu, C. N., Kappel, C., Keller, B., Sicard, A., Takebayashi, Y., Breuninger, H., Nowak, M. D., Bäurle, I., Himmelbach, A., Burkart, M., Ebbing-Lohaus, T., Sakakibara, H., Altschmied, L., Conti, E., & Lenhard, M. (2016). Presence versus absence of *CYP734A50* underlies the style-length dimorphism in primroses. *eLife*, *5*, e17956.

Huu, C. N., Plaschil, S., Himmelbach, A., Kappel, C., & Lenhard, M. (2022). Female self-incompatibility type in heterostylous *Primula* is determined by the brassinosteroid-inactivating cytochrome P450 CYP734A50. *Current Biology*, *32*, 671-676.e5.

Innes, P. A., Smart, B. C., Barham, J. A. M., Hulke, B. S., Kane, N. C. (2023). Chromosome-scale genome assembly of lewis flax (*Linum lewisii* Pursh.) bioRxiv 2023.10.10.561607; doi: https://doi.org/10.1101/2023.10.10.561607

Korunes, K. L., Samuk, K. (2021). pixy: Unbiased estimation of nucleotide diversity and divergence in the presence of missing data. *Molecular Ecology Resources*, *21*, 1359–1368.

Kumar, S., Stecher, G., Li, M., Knyaz, C., & Tamura, K. (2018). MEGA X: Molecular Evolutionary Genetics Analysis across Computing Platforms. *Molecular Biology and Evolution*, *35*, 1547–1549.

Kurtz, S., Phillippy, A., Delcher, A.L. et al. (2004). Versatile and open software for comparing large genomes. *Genome Biology*, *5*, R12.

Laenen, B., Tedder, A., Nowak, M.D., Toräng, P., Wunder, J., Wötzel, S., Steige, K.A., Kourmpetis, Y., Odong, T., Drouzas, A.D., Bink, M., Ågren, J., Coupland, G. & Slotte, T. 2018. Demography and mating system shape the genome-wide impact of purifying selection in *Arabis alpina*. *Proceedings of the National Academy of Sciences of the USA* 115: 816-821.

Laibach, F. (1923). Die Abweichungen vom ‘‘mechanischen’’ Zahlenverhältnis der Long- under Kurz-griffel bei heterostylen Pflanzen. *Biologisches Zentralblatt*, 43, 148–157.

Larsson, A. (2014). AliView: A fast and lightweight alignment viewer and editor for large datasets. *Bioinformatics*, *30*, 3276–3278.

Li, H. (2013). Aligning sequence reads, clone sequences and assembly contigs with BWA-MEM. arXiv preprint, arXiv:1303.3997.

Li, H. (2018). Minimap2: Pairwise alignment for nucleotide sequences. *Bioinformatics*, *34*, 3094–3100.

Li, J., Cocker, J. M., Wright, J., Webster, M. A., McMullan, M., Dyer, S., Swarbreck, D., Caccamo, M., Oosterhout, C. van, & Gilmartin, P. M. (2016). Genetic architecture and evolution of the *S* locus supergene in *Primula vulgaris*. *Nature Plants*, *2*, 16188.

Lloyd, D. G., & Webb, C. J. (1992). The evolution of heterostyly. In S. C. H. Barrett (Ed.), *Evolution and Function of Heterostyly* (pp. 151–178). Springer.

Love, M. I., Huber, W. Anders, S. Moderated estimation of fold change and dispersion for RNA-Seq data with DESeq2. (2014). *Genome Biology*, *15*, 550.

Löytynoja, A., Goldman, N. (2010). webPRANK: a phylogeny-aware multiple sequence aligner with interactive alignment browser. *BMC Bioinformatics*, *11*, 579.

Maguilla, E., Escudero, M., Ruíz-Martín, J., & Arroyo, J. (2021). Origin and diversification of flax and their relationship with heterostyly across the range. *Journal of Biogeography*, *48*, 1994–2007.

760 Manni, M., Berkeley, M. R., Seppey, M., Zdobnov, E. M. (2021). BUSCO: Assessing genomic data quality
761 and beyond. *Current Protocols*, *1*, e323.
762 Mattila, T. M., Laenen, B., Slotte, T. (2020). Population genomics of transitions to selfing in Brassicaceae
763 model systems. In J. Y. Dutheil (Ed.), Statistical population genomics (pp. 269–287). Springer US.
764 Mather, K., Winton, D. D. (1941). Adaptation and counter-adaptation of the breeding system in *Primula*.
765 *Annals of Botany*, *5*, 297–311.
766 Mora-Carrera, E., Stubbs, R. L., Keller, B., Léveillé-Bourret, É., de Vos, J. M., Szövényi, P., & Conti, E.
767 (2021). Different molecular changes underlie the same phenotypic transition: Origins and consequences
768 of independent shifts to homostyly within species. *Molecular Ecology*, *00*, 1– 18.
769 Mori, T., Kuroiwa, H., Higashiyama, T., & Kuroiwa T. (2006). Generative Cell Specific 1 is essential for
770 angiosperm fertilization. *Nature Cell Biology*, *8(1)*, 64-71.
771 Murray BG. 1986. Floral biology and self-incompatibility in *Linum*. *Bot Gazette* 147: 327-333.
772 Naiki, A. (2012). Heterostyly and the possibility of its breakdown by polyploidization. *Plant Species*
773 *Biology*, *27*, 3–29.
774 Nei, M., Gojobori, T. (1986). Simple methods for estimating the numbers of synonymous and
775 nonsynonymous nucleotide substitutions. *Molecular Biology and Evolution*, *3*, 418–426.
776 Page, J. T., Liechty, Z. S., Huynh, M. D., Udall, J. A. (2014). BamBam: Genome sequence analysis tools for
777 biologists. *BMC Research Notes*, *7*, 829.
778 Paradis, E. 2010. pegas: An R package for population genetics with an integrated-modular approach.
779 *Bioinformatics*, *26*, 419–420.
780 Pastor, J., Diosdado, J. C., Santa Bárbara, C., Vioque, J., & Pérez, E. (1990). Números cromosómicos para la
781 flora Española: 556-619. *Lagascalia*, *15*, 271–274.
782 Pertea, M., Pertea, G. M., Antonescu, C. M., Chang, T. C., Mendell, J. T., Salzberg, S. L. (2015). StringTie
783 enables improved reconstruction of a transcriptome from RNA-seq reads. *Nat Biotechnology*, 3, 290–
784 295.
785 Piper, J. G., Charlesworth, B., Charlesworth, D. 1986. Breeding system evolution in *Primula vulgaris* and
786 the role of reproductive assurance. *Heredity*, *56*, 207-217.
787 Pickrell, J. K., Pritchard, J. K. (2012). Inference of population splits and mixtures from genome-wide allele
788 frequency data. *PLOS Genetics*, *8*, e1002967.
789 Quesneville, H. (2020). Twenty years of transposable element analysis in the *Arabidopsis thaliana* genome.
790 *Mobile DNA*, *11*, 28.
791 Quinlan, A. R., Hall, I. M. (2010). BEDTools: A flexible suite of utilities for comparing genomic features.
792 *Bioinformatics*, *26*, 841–842.
793 R Core Team. (2021). *R: A language and environment for statistical computing.* R Foundation for Statistical
794 Computing. https://www.R-project.org/
795 Repplinger, M. (2009). Phylogenie und Biogeographie der Linoideae (Linaceae) – Evolution von
796 Heterostylie / Homostylie in *Linum*. PhD thesis. Johannes Gutenberg-Universität, Mainz, Germany.

Roessler, K., Muyle, A., Diez, C. M., Gaut, G. R. J., Bousios, A., Stitzer, M. C., Seymour, D. K., Doebley, J. F., Liu, Q., Gaut, B. S. (2019). The genome-wide dynamics of purging during selfing in maize. *Nature Plants*, 5, 980–990.

Roach, M. J., Schmidt, S. A., & Borneman, A. R. (2018). Purge Haplotigs: Allelic contig reassignment for third-gen diploid genome assemblies. *BMC Bioinformatics*, *19*, 460.

Ruiz-Martín, J., Santos-Gally, R., Escudero, M., Midgley, J. J., Pérez-Barrales, R., & Arroyo, J. (2018). Style polymorphism in *Linum* (Linaceae): A case of Mediterranean parallel evolution? *Plant Biology*, *20 Suppl 1*, 100–111.

Shimizu, K. K., Tsuchimatsu, T. 2015. Evolution of selfing: recurrent patterns in molecular adaptation. *Annual Review of Ecology, Evolution, and Systematics*, 46, 593–622.

Shore, J. S., Hamam, H. J., Chafe, P. D. J., Labonne, J. D. J., Henning, P. M., & McCubbin, A. G. (2019). The long and short of the *S*-locus in *Turnera* (Passifloraceae). *New Phytologist*, *224*, 1316–1329.

Slotte, T., Foxe, J. P., Hazzouri, K. M., Wright, S. I. (2010). Genome-wide evidence for efficient positive and purifying selection in *Capsella grandiflora*, a plant species with a large effective population size. *Molecular Biology and Evolution*, *27*, 1813–1821.

Slotte, T., Hazzouri, K., Ågren, J. et al. (2013). The *Capsella rubella* genome and the genomic consequences of rapid mating system evolution. *Nature Genetics*, *45*, 831–835.

Slotte, T. (2014). The impact of linked selection on plant genomic variation. *Briefings in Functional Genomics*, *13*, 268–75.

Smit, A. F. A., & Hubley, R. (2008). *RepeatModeler*. https://www.repeatmasker.org/RepeatModeler/

Smit, A. F. A., Hubley, R., & Green, P. (2013). *RepeatMasker* (v.4.1.0). https://www.repeatmasker.org/

Stebbins, G. L. (1957). Self-fertilization and population variability in the higher plants. *The American Naturalist*, *91*, 337–354.

Stecher, G., Tamura, K., & Kumar, S. (2020). Molecular Evolutionary Genetics Analysis (MEGA) for macOS. *Molecular Biology and Evolution*, *37*, 1237–1239.

Tataru, P., Mollion, M., Glémin, S., Bataillon, T. (2017). Inference of distribution of fitness effects and proportion of adaptive substitutions from polymorphism data. *Genetics*, *207*, 1103–1119.

Thorvaldsdóttir, H., Robinson, J. T., Mesirov, J. P. (2013). Integrative Genomics Viewer (IGV): high-performance genomics data visualization and exploration. *Briefings in Bioinformatics*, *14*, 178-192.

Tsuchimatsu, T., Suwabe, K., Shimizu-Inatsugi, R., Isokawa, S., Pavlidis, P., Städler, T., Suzuki, G., Takayama, S., Watanabe, M., Shimizu, K. K. (2010). Evolution of self-compatibility in Arabidopsis by a mutation in the male specificity gene. *Nature*, 464, 1342-1346.

Tsuchimatsu, T., Kaiser, P., Yew, C. L., Bachelier, J. B., Shimizu, K. K. Recent loss of self-incompatibility by degradation of the male component in allotetraploid *Arabidopsis kamchatica*. (2012). *PLoS Genetics*, *8*, e1002838.

Tsuchimatsu, T., Shimizu, K. K. (2013). Effects of pollen availability and the mutation bias on the fixation of mutations disabling the male specificity of self-incompatibility. *Journal of Evolutionary Biology*, *26*, 2221–2232.

835 Tsukamoto, T., Ando, T., Takahashi, K., Omori, T., Watanabe, H., Kokubun, H., Marchesi, E., Kao, T. H.
836 (2003). Breakdown of self-incompatibility in a natural population of *Petunia axillaris* caused by loss of
837 pollen function. *Plant Physiology*, *131*, 1903–1912.
838 Uyenoyama, M. K., Zhang, Y., Newbigin, E. (2001). On the origin of self-incompatibility haplotypes:
839 transition through self-compatible intermediates. *Genetics*, *157*, 1805–1817.
840 Walker, B. J., Abeel, T., Shea, T., Priest, M., Abouelliel, A. et al. (2014) Pilon: an integrated tool for
841 comprehensive microbial variant detection and genome assembly improvement. *PLoS ONE*, *9*, e112963.
842 Wang, X.-J., Barrett, S. C. H., Zhong, L., Wu, Z.-K., Li, D.-Z., Wang, H., & Zhou, W. (2021). The genomic
843 selfing syndrome accompanies the evolutionary breakdown of heterostyly. *Molecular Biology and*
844 *Evolution*, *38*, 168–180.
845 Weir, B. S., Cockerham, C. C. (1984). Estimating F-statistics for the analysis of population structure.
846 *Evolution*, *38*, 1358–1370.
847 Williamson, R. J., Josephs, E. B., Platts, A. E., Hazzouri, K. M., Haudry, A., et al. (2014) Evidence for
848 widespread positive and negative selection in coding and conserved noncoding regions of *Capsella*
849 *grandiflora*. *PLOS Genetics*, *10*, e1004622.
850 Wright, S. (1951). The genetical structure of populations. *Annals of Eugenics*, *15*, 323–354.
851 Wright, S. (1969). Evolution and the genetics of populations. In *The theory of gene frequencies. Vol 2.*
852 (University of Chicago Press.).
853 Wright, S. I., Kalisz, S., & Slotte, T. (2013). Evolutionary consequences of self-fertilization in plants.
854 *Proceedings of the Royal Society B: Biological Sciences*, *280*, 1760.
855 Wright, S. I., Ness, R. W., Foxe, J. P., Barrett, S. C. H. (2008). Genomic consequences of outcrossing and
856 selfing in plants. *International Journal of Plant Sciences*, *169*, 105–118.
857 Yasui, Y., Mori, M., Aii, J., Abe, T., Matsumoto, D., Sato, S., Hayashi, Y., Ohnishi, O., Ota, T. (2012). *S-*
858 *LOCUS EARLY FLOWERING 3* is exclusively present in the genomes of short-styled buckwheat plants
859 that exhibit heteromorphic self-incompatibility. PLoS One, 7, e31264.
860 Yang, J., Xue, H., Li, Z., Zhang, Y., Shi, T., He, X., Barrett, S. C. H., Wang, Q., Chen, J. (2023). Haplotype-
861 resolved genome assembly provides insights into the evolution of *S*-locus supergene in distylous
862 *Nymphoides indica*. *New Phytologist*, In press.
863 Yi, H., Wang, J., Wang, J., Rausher, M., Kang, M. (2022). Genomic insights into inter- and intraspecific
864 mating system shifts in *Primulina*. *Molecular Ecology*. 31, 5699–5713.
865 Yuan, S., Barrett, S. C. H., Duan, T., Qian, X., Shi, M., Zhang, D. (2017). Ecological correlates and genetic
866 consequences of evolutionary transitions from distyly to homostyly. *Annals of Botany*, *120*, 775–789.
867 Zhao, Z., Zhang, Y., Shi, M., Liu, Z., Xu, Y., Luo, Z., Yuan, S., Tu, T., Sun, Z., Zhang, D. and Barrett,
868 S.C.H. (2023). Genomic evidence supports the genetic convergence of a supergene controlling the
869 distylous floral syndrome. *New Phytologist*, *237*, 601–614.
870 Zhong, L., Barrett, S. C. H., Wang, X.-J., Wu, Z.-K., Sun, H.-Y., Li, D.-Z., Wang, H., & Zhou, W. (2019).
871 Phylogenomic analysis reveals multiple evolutionary origins of selfing from outcrossing in a lineage of
872 heterostylous plants. *New Phytologist, 224*, 1290–1303.

873 **Tables**

874

875 **Table 1.** Sequence divergence between *L. trigynum* and *L. tenue* genome assemblies at the five homologous
876 genes they share in the *S*-locus region. Synonymous and nonsynonymous substitution rates are indicated by
877 d_S and d_N, respectively. Standard errors (SE) of both are given as well as the number of major-effect
878 mutations.

Gene	n_{Ltri}[1]	n_{Lten}[2]	d_S	SE_{dS}	d_N	SE_{dN}	Coding sites	Major-effect
LITEG00000052183	3	4	0.10	0.034	0.018	0.007	176	0
indelg2	3	6	0.036	0.023	0.073	0.020	86	0
LtTSS1	3	8	0.021	0.015	0.006	0.004	144	Segregating premature stop
LtWDR-44	3	8	0.017	0.005	0.012	0.002	925	0
LtTPR LITEG00000052188	3	5	0.018	0.010	0.009	0.004	267	0

879 [1]Sample size, *L. trigynum,* [2]Sample size, *L. tenue*

880

881 **Figures**

882

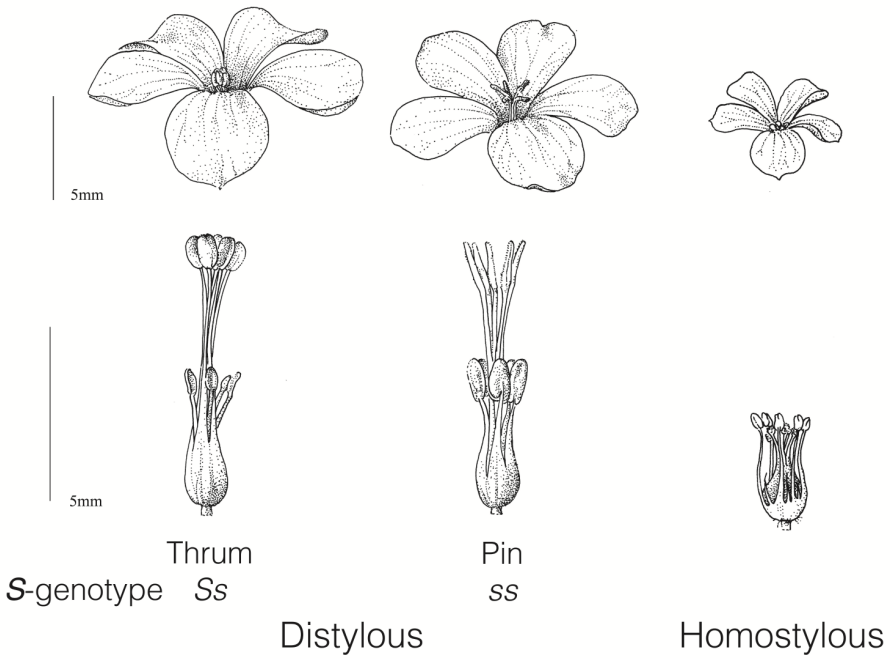

883

884

885 **Fig. 1. Flower morphs of the distylous *L. tenue* and the homostylous *L. trigynum*.** The expected
886 genotypes of thrum, pin and homostylous flowers are indicated. *S*= dominant haplotype, *s*=recessive
887 haplotype, and *S**= haplotype homologous to the *L. tenue S* allele. Illustrations by Alison Cutts.

888

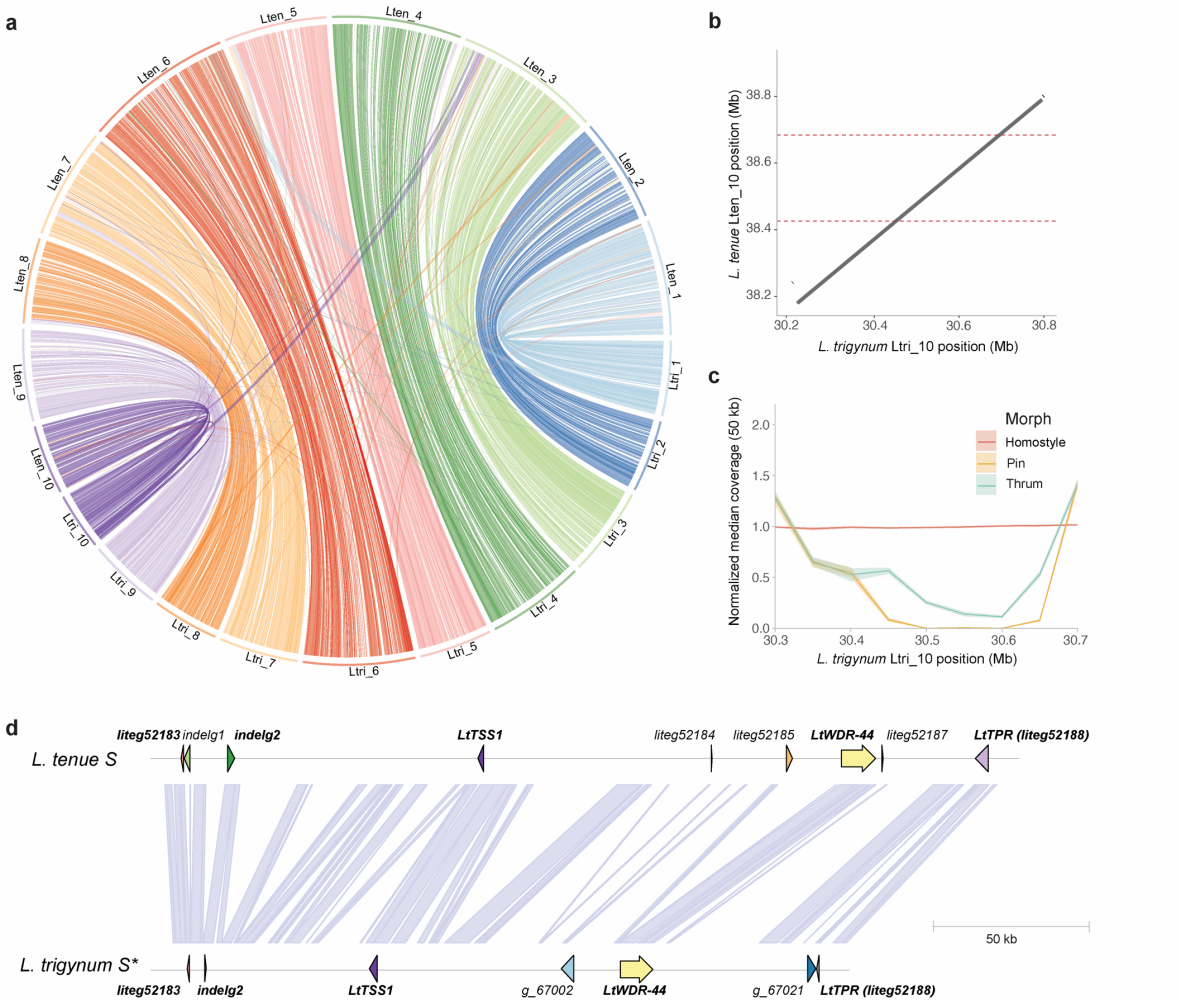

Fig. 2. Broad-scale synteny between *L. trigynum* and *L. tenue* and comparative analyses of the *S*-locus region. (a) Circos plot showing broad-scale synteny between *L. tenue* (top) and *L. trigynum* (bottom). **(b)** Dotplot showing significant minimap2 alignments between the genomic region harboring the dominant *S*-haplotype of *L. tenue* and a region of *L. trigynum* chromosome 10. The limits of the *L. tenue S*-locus are indicated by dotted lines. **(c)** Plot of median and 95% confidence intervals of median coverage in 50 kb windows for *L. trigynum* (homostyle), *L. tenue* thrum and pin individuals, all mapped to our *L. trigynum* assembly. **(d)** Comparison of gene content at the *S*-haplotype of *L. tenue* and corresponding region (here named *S**) in *L. trigynum*. Names of genes shared between the *L. tenue S*-haplotype and the *L. trigynum S**-haplotype are written in bold text.

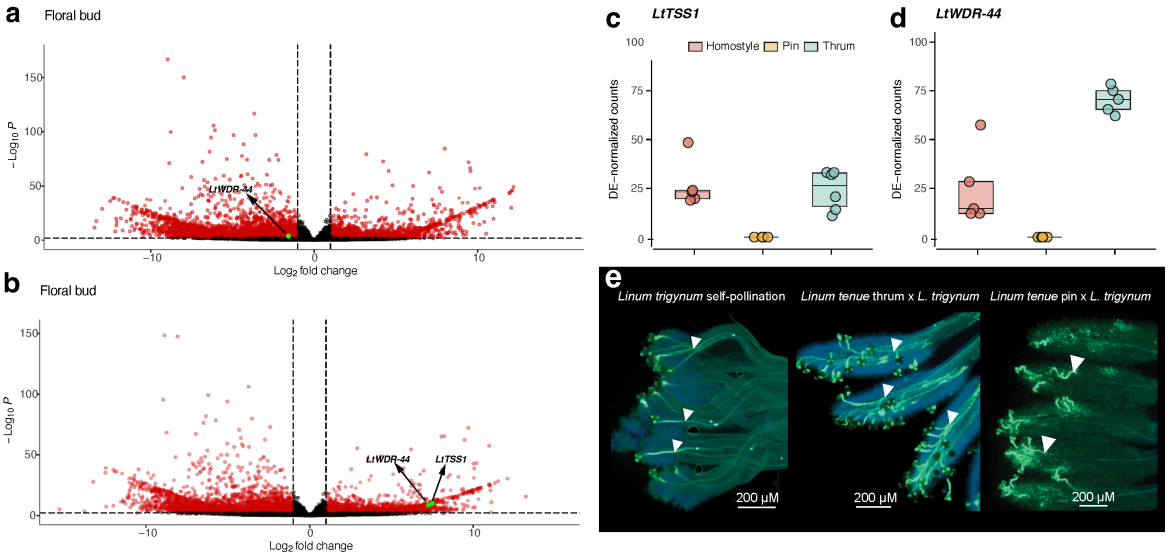

Fig. 3. Differential expression of *S*-linked candidate genes in floral buds and pollination assays suggest a role for downregulation of *LtWDR-44* in transition to homostyly. (a) Volcano plot depicting fold change vs significance of differential expression between *L. trigynum* homostyles and *L. tenue* thrums. Significant *S*-linked genes (only *LtWDR-44* in this analysis) are indicated. (b) Volcano plot depicting fold change vs significance of differential expression between *L. trigynum* homostyles and *L. tenue* pins. Significant *S*-linked genes (*LtWDR-44* and *LtTSS1*) are indicated. (c) Normalized counts for *LtTSS1* in *L. trigynum* homostyles, *L. tenue* pins and *L. tenue* thrums. (d) Normalized counts for *LtWDR-44* in *L. trigynum* homostyles, *L. tenue* pins and *L. tenue* thrums. (e) Representative epifluorescence micrographs of pollination assays demonstrating self-compatibility of *L. trigynum* (left), a compatible reaction when pollinating *L. tenue* thrum (middle) but not pin (right) with *L. trigynum* pollen. Pollen tubes are indicated by white arrows. Note that the site of pollen tube rejection is in the style in *Linum*, such that an incompatible cross yields shorter, aborted pollen tubes. Scale bars indicate the degree of magnification.

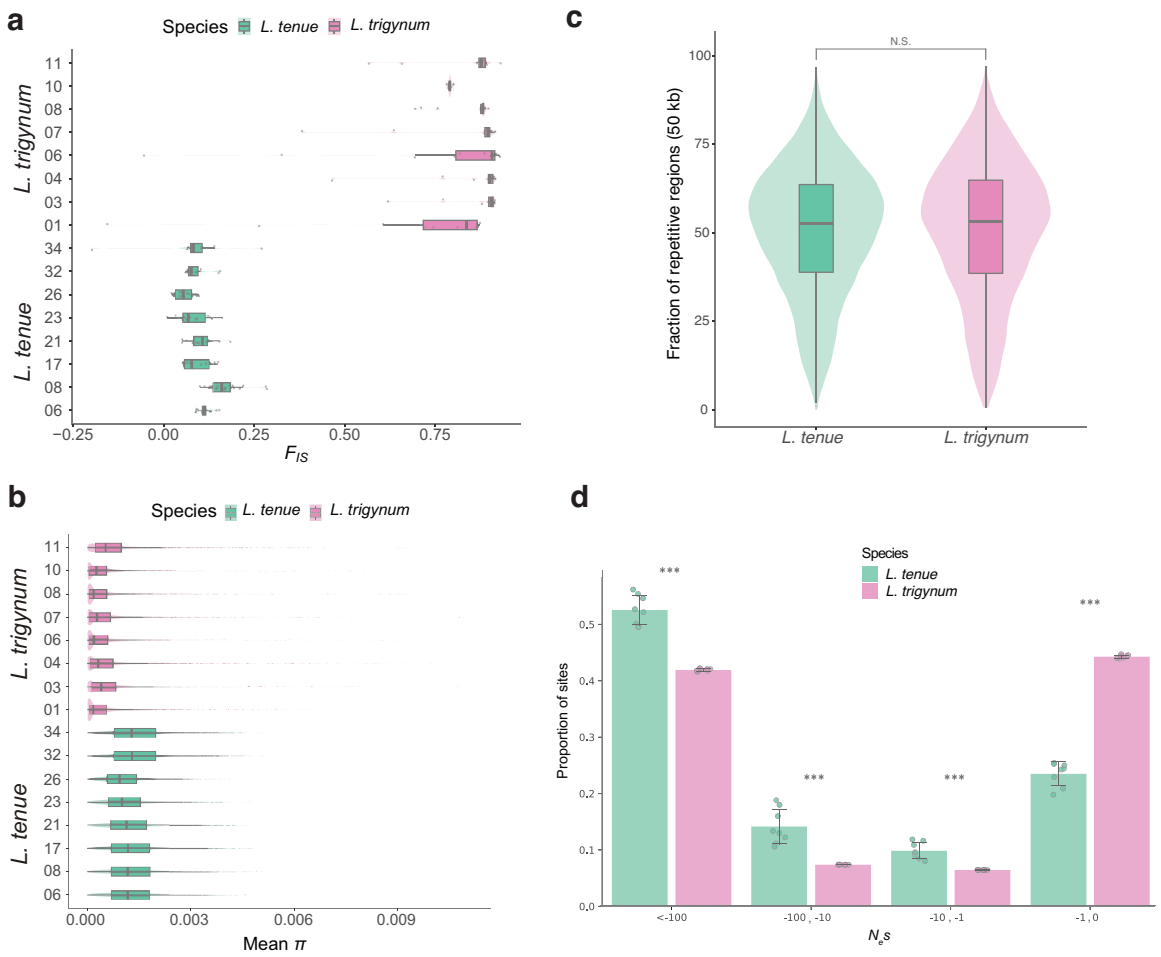

Fig. 4. The shift to homostyly in *L. trigynum* is associated with higher levels of inbreeding and marked effects on population genomic variation. (a) Inbreeding coefficient (F_{IS}) estimates for *L. trigynum* and *L. tenue* indicate higher inbreeding in *L. trigynum.* **(b)** Comparisons of π estimates in windows of 100 kb across the genome show drastically lower nucleotide diversity in *L. trigynum* compared to *L. tenue* populations. **(c)** Estimates of the percentage of TE-derived sequences in 50 kb windows across the genome (t-test: t=1.49, df=20561, $P > 0.05$, N.S.) shows that *L. trigynum* and *L. tenue* have similar TE content. **(d)** Comparison of genome-wide distribution of negative fitness effect estimates for 0-fold degenerate nonsynonymous mutations between *L. trigynum* (n=8) and *L. tenue* (n=8). Error bars represent the standard deviation derived from populations of each species. The fraction of mutations between species was significantly different for each category of $N_e s$ ($0 > N_e s > -1$ = effectively neutral, $-1 > N_e s > -10$ = moderately deleterious, $N_e s > 10$ $-10 > N_e s > -100$ and $N_e s < -100$ = strongly deleterious) (***$P < 0.001$, Wilcoxon rank sum test).

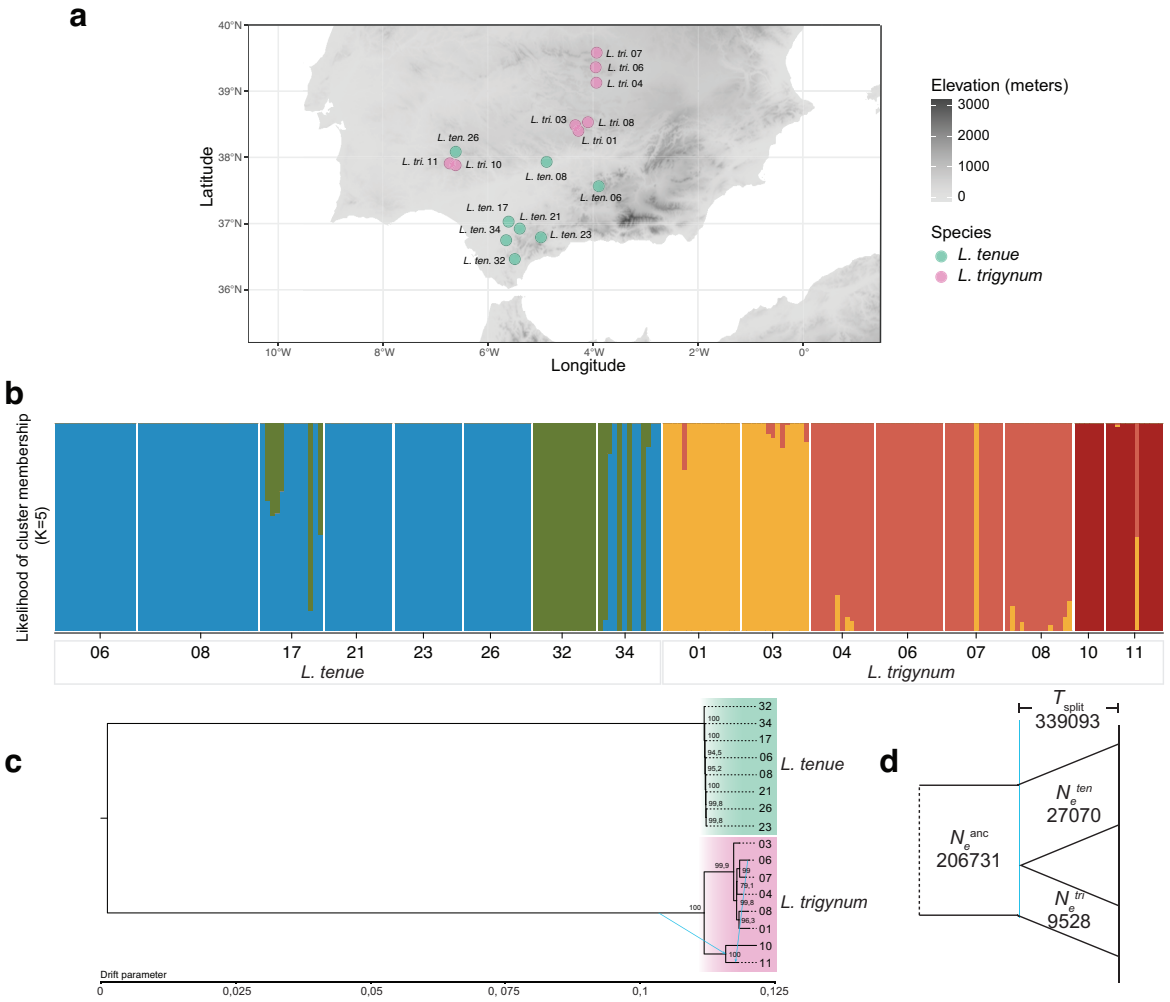

Fig. 5. Population structure and demographic history of *L. trigynum* and *L. tenue*. (a) Geographic origin of the Iberian populations of *L. trigynum* (*n*=8) and *L. tenue* (*n*=8) included in this study. **(b)** Assignment of individuals to each of the five inferred ancestral clusters (*K*=5) based on admixture models to describe population structure in ADMIXTURE. **(c)** Maximum likelihood tree inferred by TreeMix. Bootstrap values for each bifurcation and two migration edges within *L. trigynum* are shown. **(d)** The demographic model inferred by dadi. Estimates of ancestral and current effective population sizes (in numbers of individuals) and the time of the split (in number of generations) are shown.